Automated environmental mineralogy; the use of liberation analysis in humidity cell testwork

Brough, C[1*]., Strongman, J[1]., Bowell, R[2]., Warrender, R.[2], Prestia, A[3], Barnes, A[4]. Fletcher, J[1].

1. *Petrolab Limited, C Edwards Offices, Gweal Pawl, Redruth, Cornwall, TR15 3AE*
2. *SRK Consulting (UK) Ltd, 5th Floor, Churchill House, 17 Churchill Way, Cardiff, CF10 2HH*
3. *SRK Consulting US Inc., Suite 300, 5250 Neil Road, Reno, NV, 89502, USA*
4. *Geochemic Ltd, Abergavenny, Wales*

**Corresponding Author: chris@petrolab.co.uk*

Abstract

As part of the assessment of acid rock drainage and metal leaching (ARDML) potential, kinetic humidity cell tests (HCTs) are used to simulate accelerated weathering in order to predict the long-term geochemical behaviour of future mine waste material. These tests are run for a minimum of 20 weeks (ASTM, 2013) and often for in excess of 100 weeks. One of the key challenges of HCTs is the determination of cell termination. This is particularly true where there are discrepancies in prediction between static and kinetic tests, for example when corresponding static geochemical tests have predicted a significant acid-generation potential but the HCT leachate has been circum-neutral, even after 100+ weeks of testing.

One response to this uncertainty is to run HCTs for extended durations to empirically demonstrate a lack of acid generation. However, this costs substantial time and money. This paper explores a mineralogical response to the uncertainty by undertaking quantitative liberation analysis on sulfide minerals from pre-leach HCT material. The results show that pyrite liberation analysis can determine which HCTs contain a significant degree of sulfide encapsulation and therefore need to be run for prolonged periods of time. This information could also be used to increase confidence in the earlier termination of cells which contain no significant sulfide encapsulation. Altogether, quantitative liberation analysis opens up to possibility of saving time and money and improving the overall quality of a geochemical program.

Introduction

The weathering and gradual oxidation of exposed sulfides in mine waste material has the potential to result in acid-rock drainage and metal(loid) leaching (ARDML). If the potential for ARDML is not identified during the early stages of mine planning and design, it can result in serious environmental liability and unforeseen closure costs in waste management plans that are not appropriately designed. Further development of acid conditions can also impact metallurgical performance, for example in the heap leaching of transitional and sulfide facies heap leach ore.

For this reason the accurate assessment of ARDML risk now forms a critical part of Pre-Feasibility and Feasibility level mine design evaluations. It is also a requirement of the Equator Principles governing Environmental and Social Impact Assessment and permitting on projects funded by the World Bank. Guidance on ARDML assessment is published in the Global Acid Rock Drainage Guide (GARD Guide, 2014) with more specific and detailed tests reported in the MEND report (2009). Outlined in these reports are the procedures for static (short-term) and kinetic (long-term) geochemical characterisation tests. Kinetic tests in particular are one of the key tools for predicting the long-term weathering of mine waste materials. Kinetic tests are designed to accelerate and mimic field-based oxidation, which along with suitable quantitative modelling and scaling allows for the prediction of future water quality from mine sites (e.g. Frostad et al., 2002; Lapakko, 2003; Bezaazoua et al., 2004). One of the most widely used standard kinetic test procedures is the humidity cell test (HCT) (Sapsford et al., 2009; ASTM, 2013). This test requires a significant time period to generate representative data, with typical test duration in excess of 40 weeks (Barnes et al., 2015).

Static tests define the ARDML potential of any given material type through various test protocols such as acid-base accounting (ABA), net-acid generation (NAG) tests and whole rock assays (WRA). Static tests can also be carried out on pulped material. In contrast kinetic tests require percolation so tend to use a coarser material and are completed on crushed material (typically -6.3mm) material. The difference in particle size-distributions frequently result in discrepancies between the ARDML potential predicted by static tests and kinetic tests. These differences are related to textural and mineralogical controls, with factors such as encapsulation, grain size, crystallinity, galvanic decoupling and mineralogy all affecting the rate of constituent release and/or acid-generation (e.g. Thornber, 1993; Lehner et al., 2007; Lottermoser, 2010; Payant et al., 2011; Brough et al., 2013; Parbakhar-Fox et al., 2013, 2015).

One of the typical uncertainties with an HCT is how to determine when textural controls are providing a sufficient rate-limiting step such that the acid generating potential suggested by static tests will not be realised during the execution of the HCT and possibily during natural weathering over a reasonable period of time on the order of centuries or less. One possible response to this uncertainty is to run HCTs for extended lengths of time (e.g. over 100 weeks - Lapakko and Antonson, 2006) to show empirically that acid generation doesn't transpire during the test. However, this is both expensive and time-consuming and may still lead to uncertainty over the timing of acid generation which may be delayed. Alternatively the HCT could be terminated after 20 - 40 weeks with a subsequent mineralogical assessment to determine the textural reasons for the lack of ARDML. This approach also contains risks, not least that if the mineralogical study determines

no good textural or mineralogical reason for a lack of ARDML then the HCT may have been terminated too soon. At present there are no fixed criteria to determine when HCTs should be terminated and in practice it depends upon leachate chemistry data and user experience.

As an alternative or supplement to the geochemistry approach the authors here present a mineralogical approach to the issue. The use of automated mineralogy in predictive ARD studies is an emerging tool recently highlighted or applied in several publications (Goodall, 2008; Aranda et al., 2009; Parbhakar-Fox et al., 2011; Barazzoul et al., 2012; Brough et al., 2013; Becker et al., 2015). This paper aims to evaluate: (i) the use of a quantitative automated mineralogy step on pre-leach HCT material to the assessment of ARDML potential within a sample; and (ii) whether in principal a pre-leach textural assessment would aid in the decision making process of when to terminate a HCT.

Materials and Methods

Three samples representative of future mine waste from an epithermal gold deposit were submitted for static and kinetic testing. The static tests included ABA and NAG testing. ABA indicates the theoretical potential for a given material to produce net acid conditions. It determines the acid generating potential (AP) and neutralising potential (NP) of each sample based on sulfide sulfur and inorganic carbon content, respectively. ABA entails complete combustion of a sample in a Leco furnace and determination of the CO_2 and SO_2 given off from the sample.

The classification of acid generation potential is proportional to sulfide-S content of the sample. Sulfide Sulfur concentration is mass balanced to an estimate of calcium carbonate content required to neutralize acid generated by an equivalent amount of pyrite based on the stoichiometric relationship for reaction [1].

$$FeS_2 + 2CaCO_3 + 3.5H_2O + 3.75O_2 = 2CaSO_4 + Fe(OH)_3 + 4H^+ + 2CO_3^{2-} \quad [1]$$

This generates an estimate of acid generating potential (mole ratio of 31.25 multiplied by sulfide S content, as a percentage converted to kg $CaCO_3$ equivalent per ton of rock required to neutralize that amount of protons). This measurement is then deducted from an estimate of Neutralization Potential. This is taken from conversion of analysed inorganic carbon and conversion to kg $CaCO_3$ equivalent per ton of rock or from titration measurements. This generates an estimate of the Net Neutralization Potential, with a negative value indicating net acidic conditions predicted. Another parameter derived is a ratio of the NP to AGP with values below 1 indicating more AGP than NP or net acidic conditions can potentially form.

Net Acid Generation (NAG) tests are slightly different and provide an estimate of the acid generated through the accelerated oxidation of sulfides by hydrogen peroxide to generate sulfuric acid. The acid produced consequently dissolves any neutralising minerals present, with the net result that acid production (NAG value as equivalent kg H_2SO_4 per ton of rock generated) and predicted final pH (NAG pH) can be measured directly. The NAG test was completed applying the method developed by EGI (2002), which involves intensive oxidation of a pulverised sample using hydrogen peroxide. For the purposes of the testwork, 2.5 g of pulverised sample was refluxed with 250 mL of hydrogen peroxide (H_2O_2) for a minimum of three hours. After the reaction was complete, a sub-sample was

collected for ICP-OES/ICP-MS analysis and remaining leachate was then titrated with sodium hydroxide (NaOH) in two stages (to pH 4.5 and to pH 7) to determine the NAG value.

The kinetic tests were carried out according to the ASTM D 5744 standard methodology (version 7, ASTM, 2013) HCT and were run for a total of 144 weeks. Under ASTM methodology, the test followed a seven-day cycle during which water is trickled over the rock to saturate the column. After draining, dry air was circulated through the cell for 3 days followed by humidified air at 25^{o}C for 3 days. On the seventh day, the sample was rinsed again with distilled water and the extracted solution was collected for analysis following filtration at 0.45 μm.

After 67 weeks of humidity cell testing, samples of the pre-leach HCT material were submitted for mineralogical analysis in order to assess whether there were any textural controls that may be affecting the observed lack of acid generation in two of the three HCT samples. Mineralogical analysis included X-Ray Diffraction analysis (XRD), optical microscopy and automated mineralogy using Scanning Electron Microscopy (SEM).

XRD analysis was carried out on the pre-leach HCT samples using a Philips PW1710 Powder Diffractometer at the Department of Earth Science, Cardiff University, UK. Bulk analyses were carried out on samples. Scans were run using Cu Kα radiation at 35kV and 40mA, between 2 and 70 °2θ at a scan speed of 0.04 °2θ/s. From the scans, phases were identified and from the peak areas, semi quantitative analysis was performed and a percentage of each phase present calculated.

Samples of the pre-leach HCT material were prepared into polished thin sections before qualitative assessment by optical petrography and quantitative textural assessment by automated mineralogy. Optical petrography was carried out on a Meiji MX9000 fitted with a mounted Canon EOS 600D housed at SRK Consulting, Cardiff. Automated mineralogy was carried out on a ZEISS EVO MA-25 scanning electron microscope fitted with one Bruker xFlash 6|60 EDX detector housed at Petrolab Ltd, Cornwall.

Analysis on the ZEISS EVO MA-25 consisted of a bright phase search plus context. The back scatter electron threshold was narrowed to focus on pyrite particles which were then selectively analysed in the context of the immediate textural association (*Figure 1*). The image processing is undertaken by means of a routine that involves first “thresholding” (setting the back scatter electron intensity) for pyrite and then dilating out from the pyrite grain into the immediate mineralogical context. Both the dilation context and the pyrite grain are analysed pixel by pixel allowing for variation in the immediate mineralogical context to be resolved. The magnification used was x80 with a step size of 8 μm.

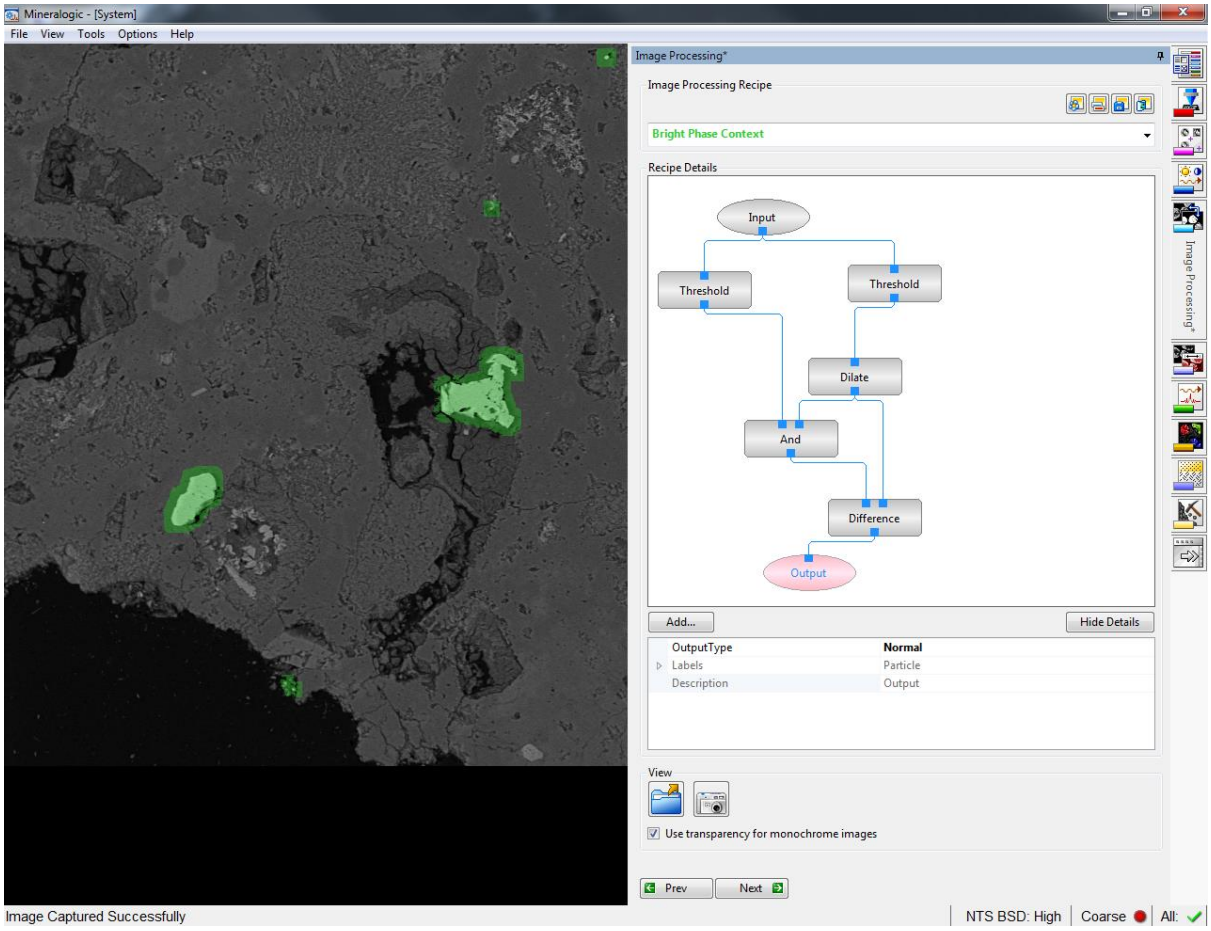

Figure 1: Image of one field from the analysis showing the analysis of pyrite grains (highlighted in light green) with an additional analysis of an immediate dilation field (in dark green) to see the immediate liberation context.

A phase classification scheme was developed using the Mineralogic Mining software. Delineating grains into different phase classes is achieved by matching criteria that compare the quantitative measurements of elemental composition, as determined from the ED spectrum, with standard mineral composition data. A mineral group name or a general name (after dominant elements) is used for a class where there is a range in the elemental composition data such that a specific mineral member cannot be separately identified (e.g. chlorite group). The speciation of all minerals was aided by data from XRD analysis and optical petrography.

Liberation, particle size data and mineral association analysis was undertaken using Mineralogic v1.3. This returns pyrite liberation analysis by partial perimeter percent by frequency in 10% bins. Additional analysis of this pyrite liberation and particle size data was carried out using mySQL modelling procedures, which returns pyrite liberation by partial perimeter adjusted for the size (area) of the pyrite grain.

Results

Static and Kinetic Tests

Static and kinetic geochemical data for the samples are summarised in Table 1 and illustrate that acid generation could be expected for all three samples based on ABA and NAG testwork results. Despite the very similar static data of the three tests the performance during kinetic testing was very different. Pre-leach 3 was producing acidic leachate from week 25, but it took until week 70 for the leachate pH to reduce to ~3.5 SI. Pre-leach 2 retained a circum-neutral pH until week 130 but produced acidic leachate very quickly from that point reducing to a pH of ~3.5 by week 145. Finally pre-leach 1 retained a circum-neutral pH for 144 weeks until its termination (*Figure 2*).

Table 1: Static test data for the samples tested

Sample	Sulfide Sulfur (%)	NNP[1] (kg $CaCO_3$ eq/t)	NPR[2]	NAG[3] pH	HCT pH at Termination	Termination Date (weeks)
Pre-Leach 1	0.85	-21.0	0.2	2.5	7.06	144
Pre-Leach 2	0.77	-19.6	0.2	2.6	3.53	Ongoing
Pre-Leach 3	0.65	-15.7	0.2	2.6	3.27	144

A graph of neutralisation potential (NP) remaining also shows three different curves for the three samples (*Figure 3*). For pre-leach 3 the NP declines to zero at a steady rate over 90 weeks. For pre-leach 2 there is a much slower decline for the first 90 weeks with a sharp increase in the rate of NP reduction after this, finally reducing to zero by week 135. For pre-leach 1 there is a slow and steady decline through to 144 weeks where there was still 78% of the NP remaining at termination.

The differences in HCT behaviour carry through to different metal(loid) release rates for the three samples (*Figure 4*). For pre-leach 3 the release of As, Co and Ni commences around 50 weeks when the pH begins to drop through the buffer at pH 5 and gradually rises through to the termination date at 144 weeks. For Zn and Pb the release starts much earlier when the pH of the solution first begins to drop and continues to rise slowly through to the termination date at 144 weeks. There was no observed Cu release in pre-leach 3. For pre-leach 2 there was no metal(loid) release until week 130 which is coincident with the initiation of the pH reduction and the subsequent metal(loid) release was rapid culminating in concentrations that were normally higher than pre-leach 3. For pre-leach 1 there was no observed increase in metal(loid) release at any point through until cell termination at 144 weeks.

[1] *NNP = Net-neutralisation potential (NP - AP). Negative numbers are potentially acid forming (PAF).*
[2] *NPR = Neutralisation potential ratio. (NP/AP). Numbers <1 are considered PAF.*
[3] *NAG = Net acid generation during accelerated weathering of pulverised material using a hydrogen peroxide leach.*

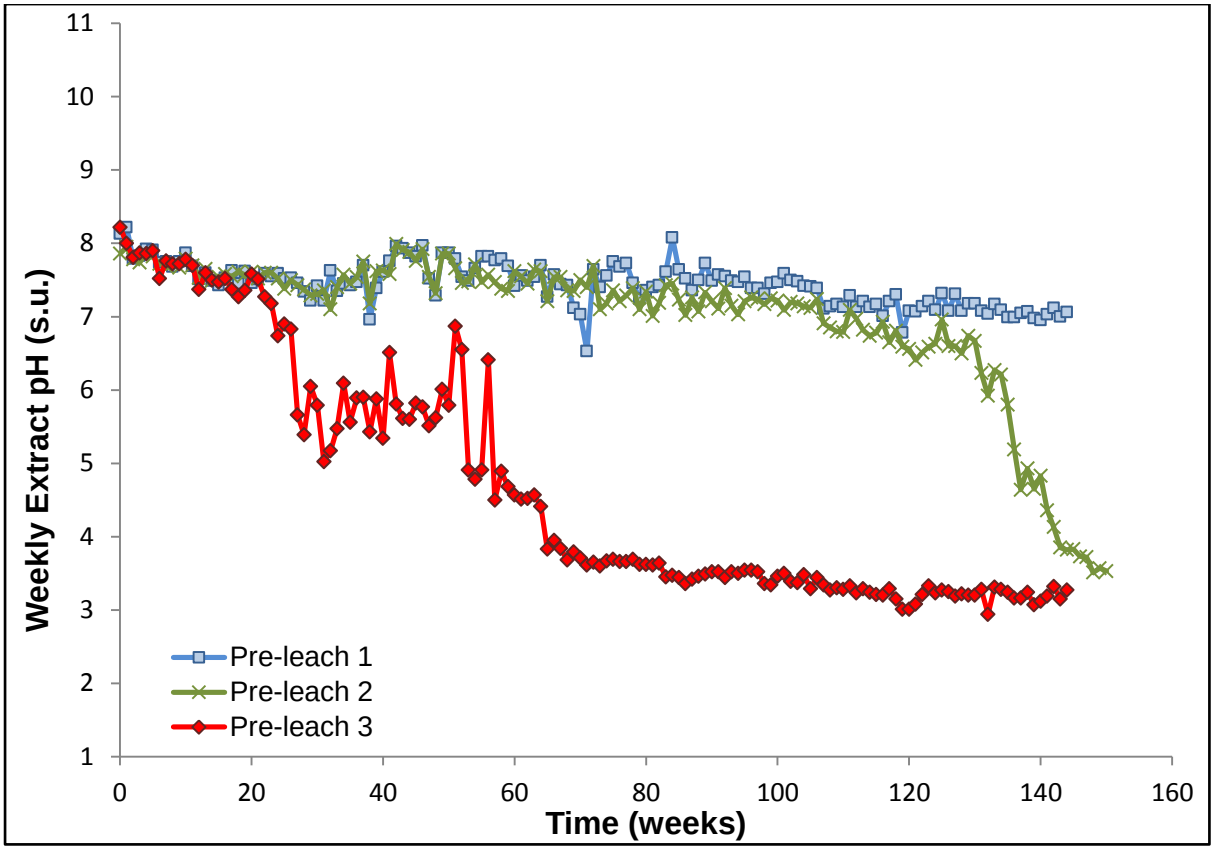

Figure 2: HCT effluent pH

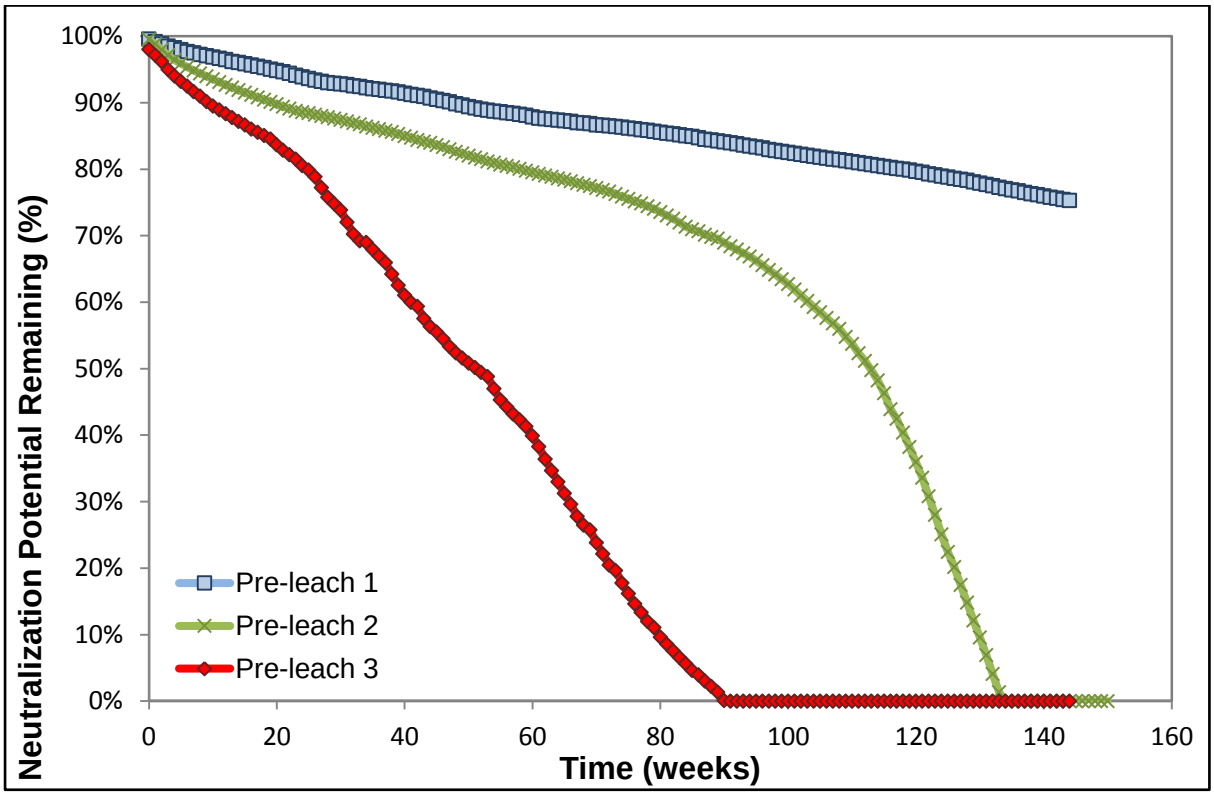

Figure 3: Neutralisation potential remaining

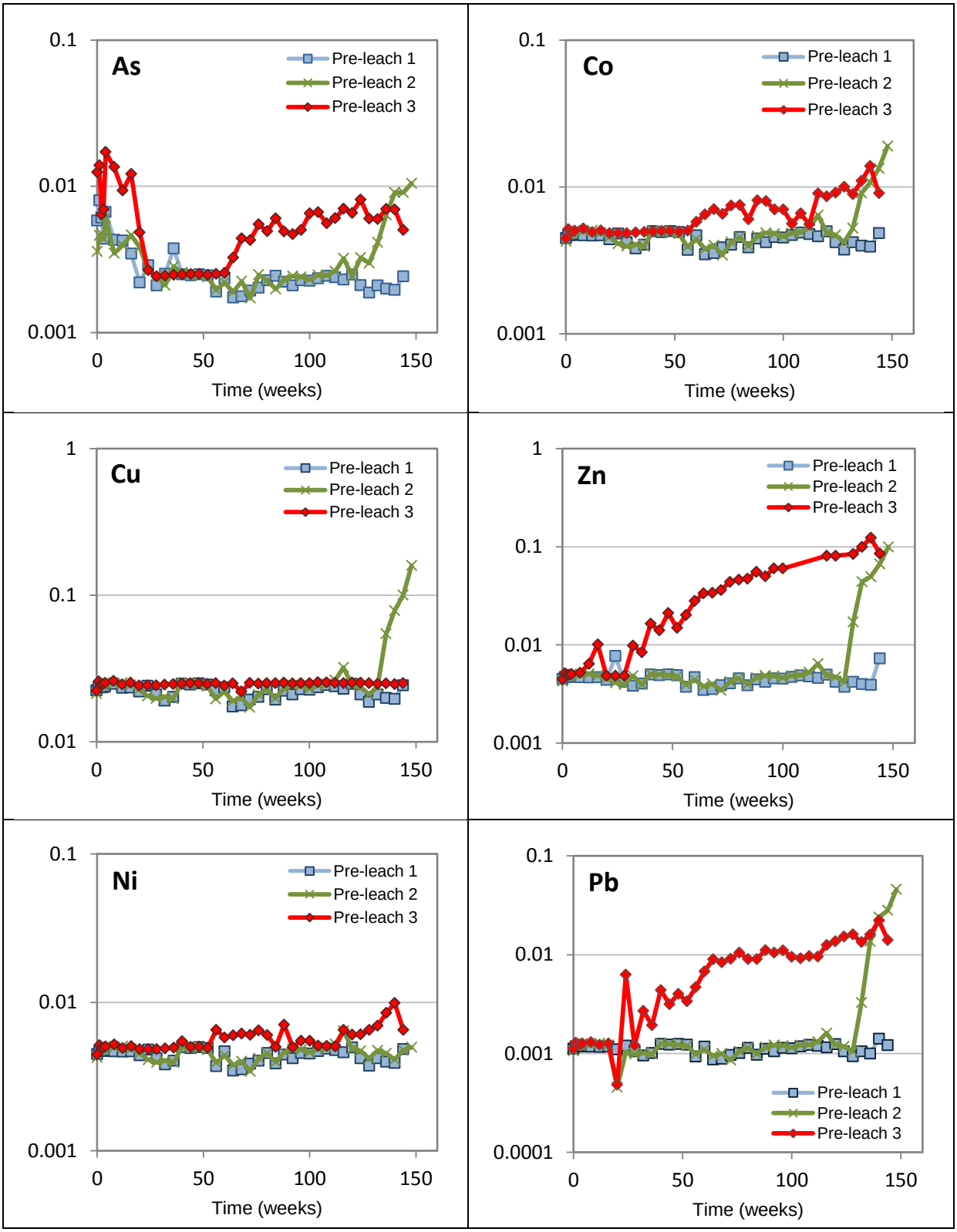

Figure 4: Metal(loid) release rate (mg/kg/week) during the HCT testwork for the three samples.

Optical Petrography & XRD

The results of the XRD analysis and optical petrography, on the pre-leach material show, that the major minerals within each sample are broadly similar (*Figure 5*). The particles predominantly consist of quartz, orthoclase and montmorillonite in association with minor amounts of illite, albite, hematite and kaolinite. Pyrite is a trace phase within all three samples as indicated by the static test results and therefore not observed in bulk XRD trace (*Figure 5*). Nevertheless the lack of carbonate minerals or ultramafic minerals is displayed (cf. Nesbitt & Jambor, 1998) and this indicates limited buffering capacity for acid for the rock types (*Table **1***)

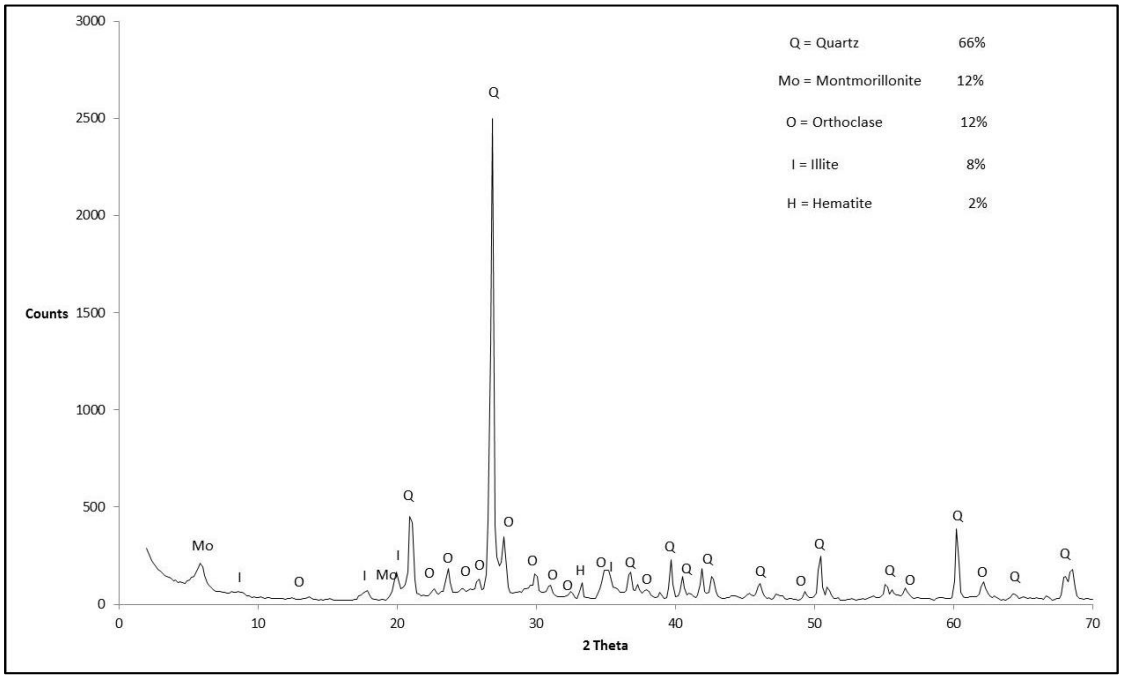

Figure 5: XRD analysis for pre-leach sample 3. Quartz peaks are marked by 'Q', whilst orthoclase peaks are marked by 'O', montmorillonite peaks by 'Mo', illite peaks by 'I' and hematite peaks by 'H'. Semi-quantitative analysis of these peaks give proportions of about 66% for quartz, 11% for montmorillonite, 9% for illite, 9% for orthoclase, 3% for kaolinite and 1% for hematite.

Qualitative textural assessment of the three samples reveals a high degree of pyrite encapsulation within non-reactive silicates (*Figure 6* & *Figure 7*). This encapsulation significantly reduces the amount of pyrite available for reaction and therefore greatly reduces the true acid-generation potential of the samples. For pre-leach sample 3 the analysis of pyrite textural developments revealed both encapsulation within non-reactive silicates and liberation (*Figure 8*) within the groundmass. Qualitatively, the degree of pyrite liberation within pre-leach 3 appeared the greatest of the three submitted samples.

*Table **2**: Table of mineral abundance from XRD analysis and optical petrography*

Mineral	**Relative Abundance**[1] **■ major (≥10%), ⊡ minor (≥1<10%), ☐ trace (<1%).**			Typical composition
	Pre-Leach 1	**Pre-Leach 2**	**Pre-Leach 3**	
Quartz	■	■	■	SiO_2
Orthoclase	■	■	⊡	$K(AlSi_3O_8)$
Montmorillonite	⊡	■	■	$(Na,Ca)_{0.33}(Al,Mg)_2(Si_4O_{10})(OH)_2.nH_2O$
Illite	⊡	⊡	⊡	$K_{0.65}Al_2[Al_{0.65}Si_{3.35}O_{10}](OH)_2$
Albite	⊡	⊡	⊡	$Na(AlSi_3O_8)$
Hematite	⊡	⊡	⊡	Fe_2O_3
Kaolinite			⊡	$Al_2(Si_2O_5)(OH)_4$
Chlorite	☐	☐	☐	$(Mg,Fe^{2+})_5Al(AlSi_3O_{10})(OH)_8$
Pyrite	☐	☐	☐	FeS_2
Zircon	☐			$ZrSiO_4$
Rutile			☐	TiO_2
Fluorapatite			☐	$Ca_5(PO_4)_3F$

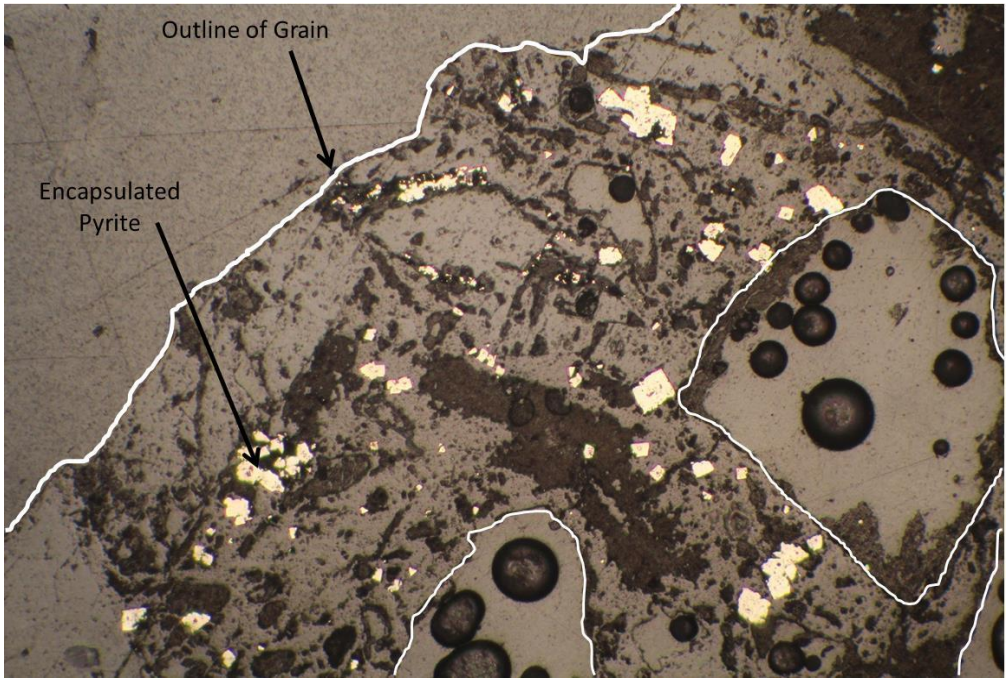

*Figure **6**: Reflected light image (Mag: x5) for pre-leach sample two. Image of a single particle showing the high degree of pyrite encapsulation present. Also apparent is the fine-grain size of the pyrite grains and euhedral to subhedral crystal development. Good crystal development will reduce the inherent reactivity of the pyrite through increased stability of the ordered lattice of the crystal.*

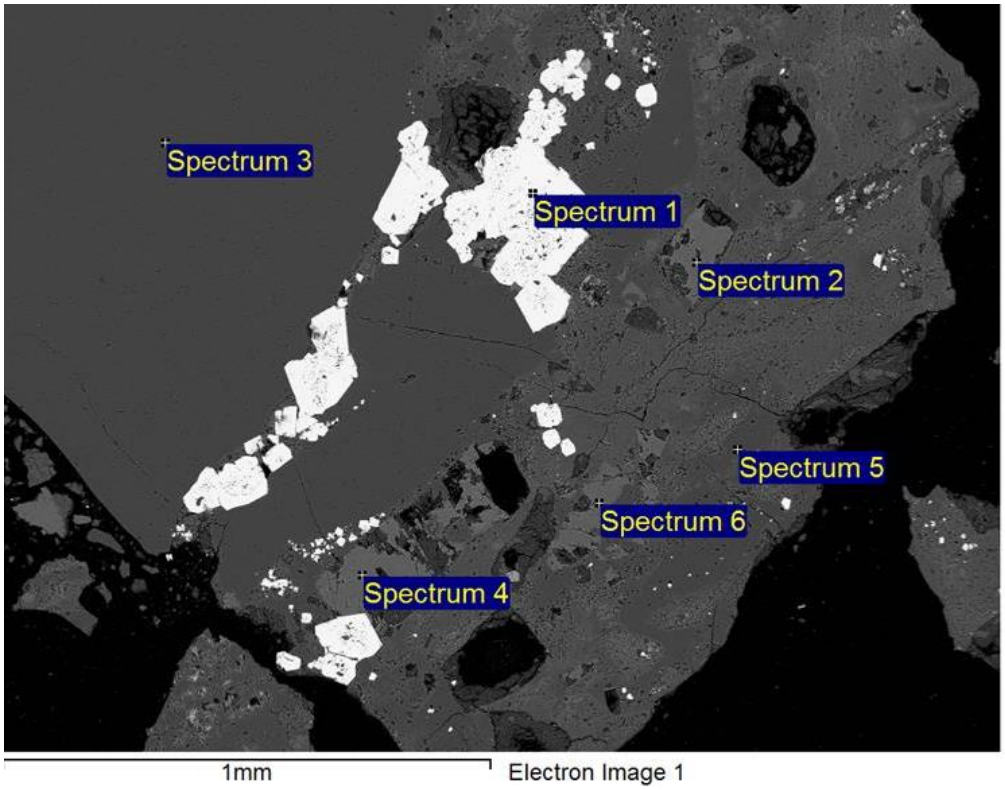

*Figure **7**: Back scatter image for pre-leach sample two. Example of coarser-grained encapsulated pyrite (Spectrum 1), associated with microcline (Spectra 2, 4 & 6) and quartz (Spectra 3 & 5).*

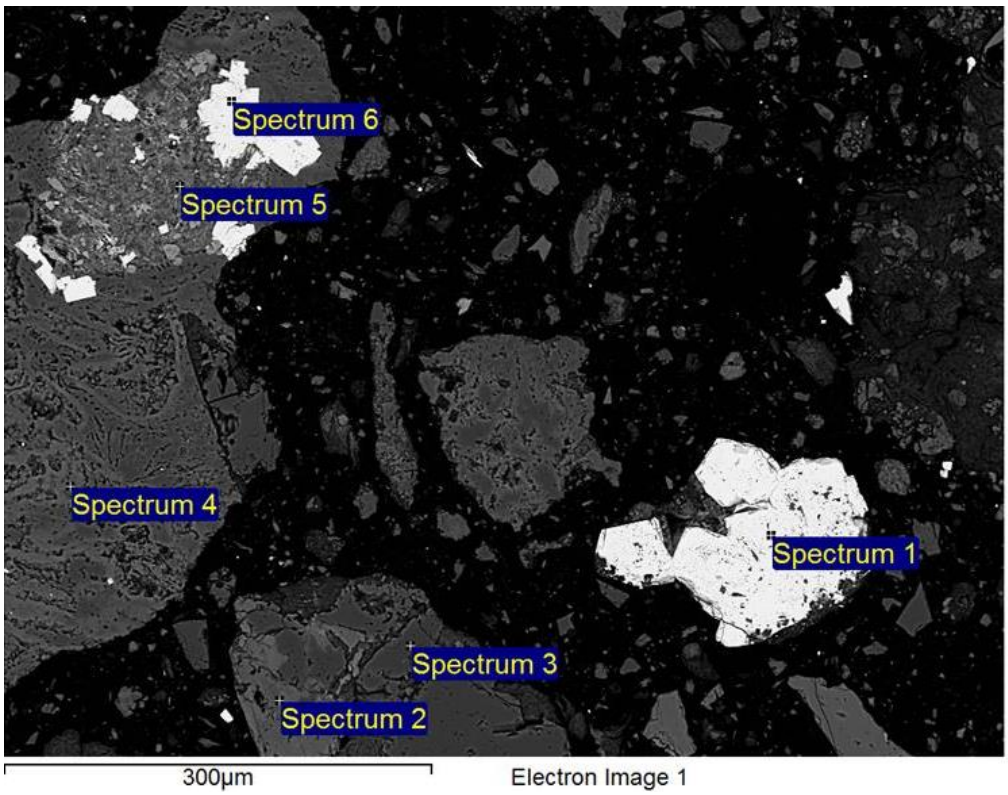

*Figure **8**: Back Scatter Image for pre-leach sample three, showing an example of liberated and encapsulated pyrite (Spectra 1 & 6), associated with microcline (Spectra 2 & 4), quartz (Spectrum 3) and a fine-grained mineral mix of illite and rutile (Spectrum 5).*

Automated Mineralogy

In addition to the information provided by optical microscopy the automated microscopy routine provides quantitative analysis of (i) the particle size distribution of pyrite; (ii) the immediate mineral associations of that pyrite and (iii) the liberation by exposed partial perimeter of the pyrite. The particle size distribution data is shown below and shows distinct differences between the three samples (*Table 3*, *Figure 9*). Pre-leach 3 contains the coarsest pyrite grains but with a similar fine pyrite size distribution to Pre-leach 1. Pre-leach 2 contains a notably finer pyrite grain size distribution. Pre-leach 3 which has the coarsest particle size distribution.

*Table **3**: Table summarising particle size distribution data for each sample*

Sample	Sulfide Sulfur from ABA (%)	Average Grain Size, ECD (µm)	Grain Size Std Deviation (µm)
Pre-leach 1	0.85	49	50
Pre-leach 2	0.77	24	31
Pre-leach 3	0.65	41	60

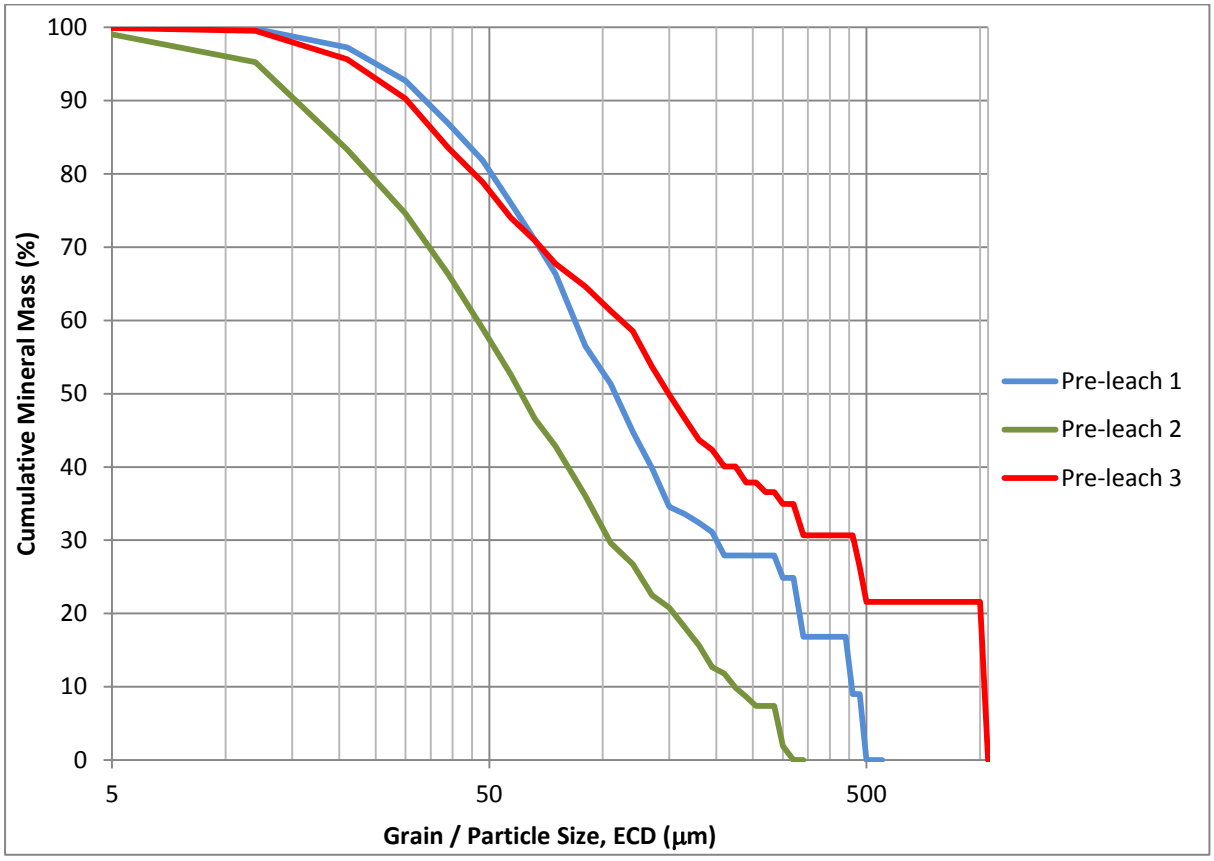

Figure 9: Particle size distributions of pyrite for each sample.

Analysis of the pyrite association data also showed strong similarities between pre-leach 1 and pre-leach 3 with similar association amounts for quartz, orthoclase, biotite, and clay minerals. For pre-leach 2 the association with quartz and orthoclase is more dominant (*Figure 10*). Despite the minor differences between the three samples it is apparent that the principal minerals associated with pyrite (>98%) for all three samples are inert non-reactive silicate phases (quartz, orthoclase, biotite and clay minerals).

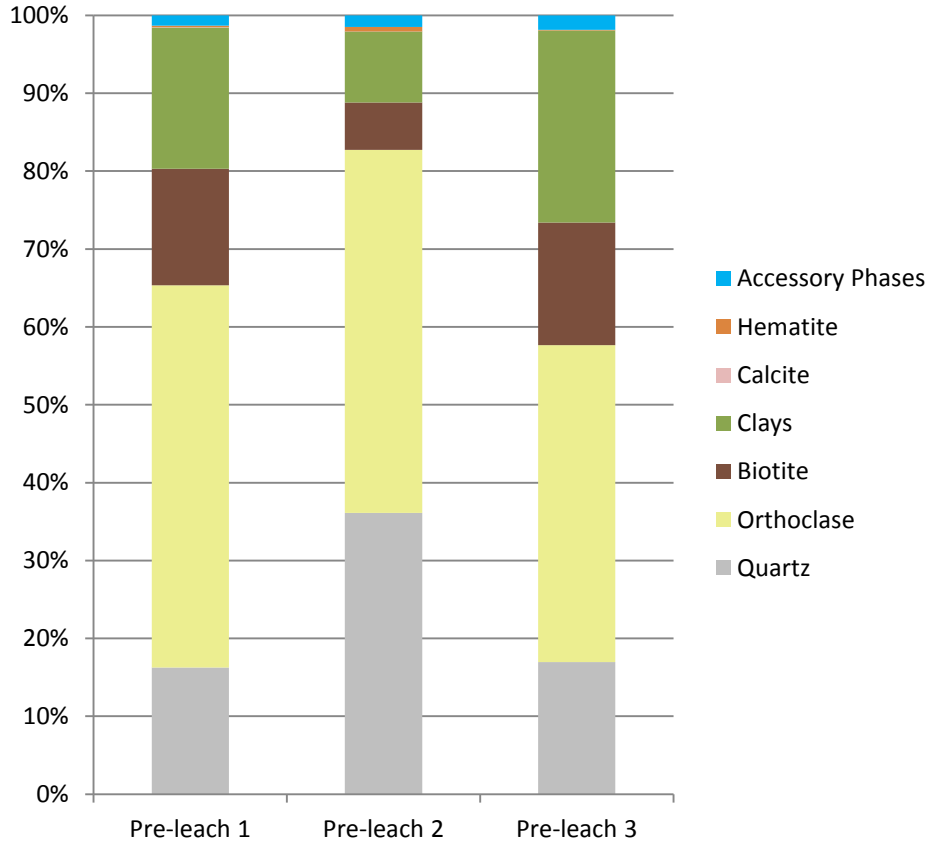

Figure 10: Mineral association data for the pyrite grains within each sample. Clays include illite, kaolinite, montmorillonite and gibbsite.

Pyrite liberation curves show the largest difference between the three leach tests. Pyrite liberation when analysed by frequency of occurrence show pre-leach 3 had the greatest degree of pyrite liberation with samples pre-leach 1 and pre-leach 2 having lower degrees of pyrite liberation (*Figure 11*). This pattern is reinforced when the pyrite liberation curves are normalised to the weight percent of pyrite in each liberation class (*Figure **12***). This method takes account of how large the pyrite grains are in each liberation class and is a more robust representation of pyrite liberation.

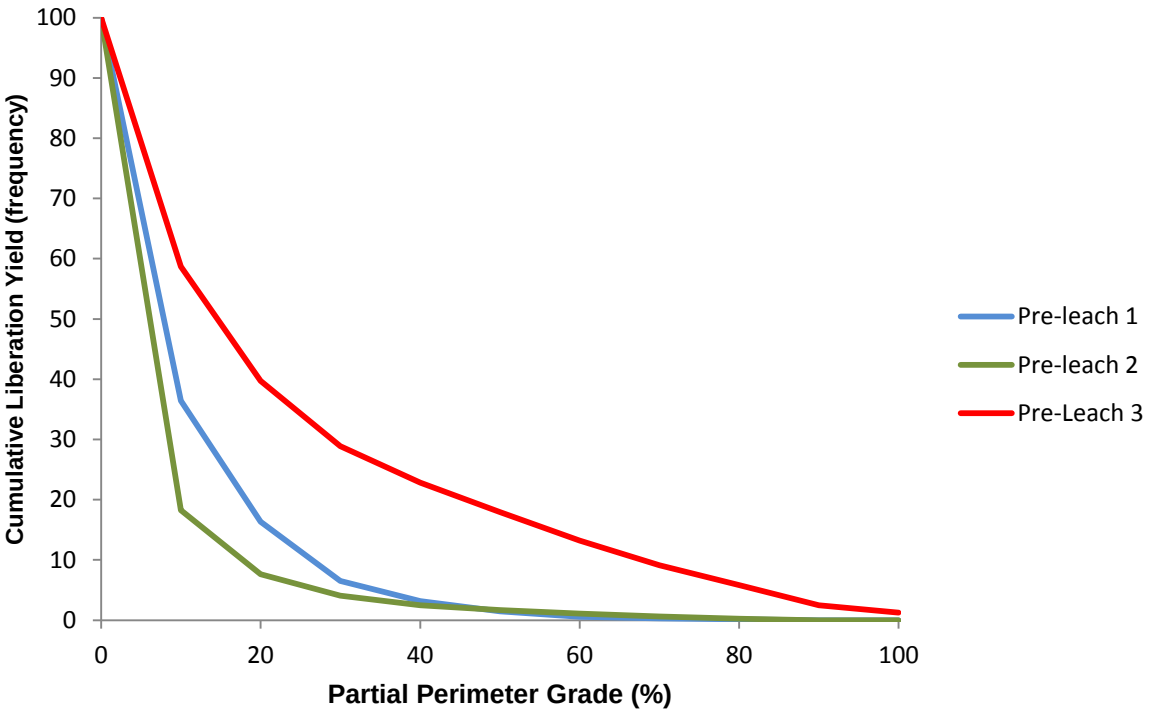

Figure 11: Cumulative liberation of pyrite calculated by frequency of pyrite grains in each liberation class.

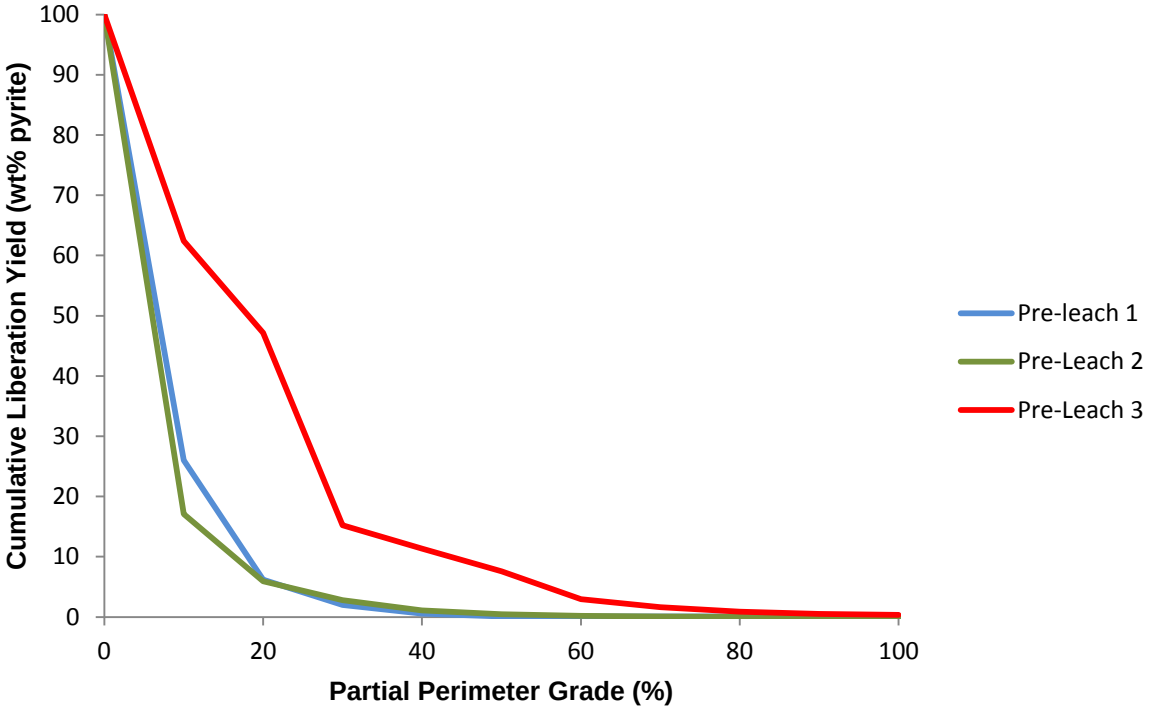

Figure 12: Cumulative liberation of pyrite calculated by weight percent of pyrite in each liberation class.

Discussion

This study has focussed on three well characterised samples where thorough static and kinetic testing was undertaken. For these three samples the sulfide sulfur contents were similar and all were predicted to be potentially acid-forming from static testwork. Two of the three samples did produce acidic leachate though after considerably different lengths of time (i.e. 25 weeks and 135 weeks), whilst the third cell had not produced acidic leachate even after 144 weeks of testing. Even the two cells that produced acidic leachate did so at very different rates. Qualitative optical petrography had provided some indication on the reasons for the difference in performance but the principal aim of this study was to ascertain whether automated liberation analysis of pyrite grains in pre-leach samples could further resolve the reasons for these differences and provide additional support to a geochemist overseeing an ARDML program.

The automated mineralogy analysis routine was undertaken using a bright phase search plus context to delimit the partial perimeters exposed for pyrite grains and their immediate mineralogical context. This analysis routine circumvents the difficulty of the coarse particle size inherent in HCT tests. As particles reach up to 6.3 mm across, coarse particles will not be resolvable within a scanning electron microscope on individual fields. By focussing the analysis on the pyrite grains with a dilation zone for immediate context it is possible to analyse the entire sample and derive accurate liberation data by partial perimeter for all the pyrite grains.

Qualitative petrographic analysis of the three samples suggested that pyrite showed a greater degree of liberation in pre-leach 3, though still with a high degree of encapsulation. Qualitatively the degree of liberation in pre-leach 1 and 2 looked similar and the magnitude of their greater encapsulation relative to pre-leach 3 was uncertain. Whilst this qualitative petrography was useful in understanding why pre-leach 3 produced acidic leachate earlier than pre-leach 1 and 2, it does not provide sufficient information to understand the difference in behaviour of pre-leach 1 and pre-leach 2, or the magnitude of the difference in behaviour of pre-leach 3 from the other two samples. This optical microscopy analysis highlights both the advantage of considering textural information in the assessment of ARD performance and the limitations of being unable to quantify these textural controls or textural differences (e.g. Parbhakar-Fox et al., 2015).

Automated Mineralogy

The automated mineralogy study quantified the liberation of the three samples and showed the degree to which pre-leach 3 had the greatest pyrite liberation, and that this was significantly higher than either pre-leach 1 or pre-leach 2 (roughly 2-3 times greater). This was true whether liberation was considered as frequency of pyrite grains in each liberation class (*Figure 11*), or as weight percent pyrite in each liberation class (*Figure 12*). This greater liberation has resulted in acid-generation whilst neutralisation potential was still remaining in the cell (cf. *Figure 3*), and this early onset acid-generation with remaining NP partly explains the long lag time between the onset of acid-generation (week 20) and a stable low-pH of ~3.5 (70 weeks). In contrast pre-leach 2 didn't produce acidic leachate until all the NP was consumed but subsequently produced acidic leachate very rapidly.

An additional observation of this liberation analysis is that all leach tests show a moderate to high degree of pyrite encapsulation, but that in the absence of neutralising carbonates or ultramafic silicate minerals even a high degree of pyrite encapsulation will not prevent acid generation during HCT testing.

The different rates of acid-generation have also had an impact of the rate of metal(loid) release with the pre-leach 3 generally showing slow and steady increase in metal(loid) loadings through to cell termination and two distinctly different start times. In contrast, pre-leach 2 showed a rapid increase in metal(loid) release for all elements that was coincident with the onset of acid-generation. This distinct behaviour in pre-leach 2 may relate to the lack of NP remaining in the cell during acid-generation but it may also relate to different trace element loadings in the pyrite. In this regard several controls on pyrite oxidation rate have been proposed for Co and Ni (which are argued to inhibit oxidation; e.g. Lehner et al., 2008) and As (which is argued to increase the rate of pyrite oxidation; e.g. Lehner et al., 2007, Lehner et al., 2008). As all elements show a rapid increase in concentration for pre-leach 2 it is currently interpreted that the increase is fundamentally controlled by the rapid oxidation of pyrite after the consumption of NP.

To further understand the difference in behaviour of pre-leach 1 and 2 requires looking at the particle size distribution (PSD) data. Analysis of pyrite PSD data showed that pre-leach 2 had the finest pyrite PSD, whilst pre-leach 3 had the coarsest pyrite PSD. Pre-leach 1 had an intermediate pyrite PSD between these two samples. Therefore, relative to pre-leach 1, pre-leach 2 has finer pyrite. This is a critical observation as their liberation curves when adjusted for weight percent are indistinguishable. Pyrite reactivity will be a function of grain shape, grain size and inclusion content (e.g. Lottermoser, 2010; Weisener & Weber, 2010) with greater reactivity for finer-grained pyrite, anhedral grains and inclusion rich pyrite. As such, the finer pyrite in pre-leach 2 will result in higher reactivity compared with the coarser pyrite in pre-leach 1 with equivalent liberation.

The association data for the three samples shows that the primary (>98%) association of pyrite in all three samples is with unreactive and stable silicate phases (quartz, orthoclase, biotite and clay minerals) and that for this project this association does not have a material effect on the pH or the metal(loid) release.

Conclusions

For these three samples the automated mineralogy study has shown that the speed with which HCT cells generate acidic leachate and release metal(loids) can be linked primarily to quantitative pre-leach pyrite liberation and secondarily to PSD data.

More generally, the principal benefits of an automated mineralogical approach is to provide valuable quantitative information on the nature of pyrite in the waste rocks which can be used to explain discrepancies between static and kinetic testwork. The quantitative nature of the analysis goes beyond optical microscopy providing both greater depth of information and greater certainty in interpretation. For the geochemist overseeing the ARDML assessment pre-leach automated tests

improve the overall quality of the geochemical program assisting in the difficult decisions of when to terminate a humidity cell or for how long to operate cells with high degrees of pyrite encapsulation.

This study opens up the possibility of further development with (i) the potential to look at carbonate liberation in conjunction with pyrite liberation, and (ii) the potential to incorporate trace element pyrite analysis through tools such as Laser ICP-MS into the interpretation of metal(loid) release. An integrated automated approach that combines state-of-the-art pyrite liberation, carbonate liberation and trace element analysis will be the focus of future ARDML assessment programs.

References

Aranda, C.A., Klein, B., Beckie, R.D., Mayer, K.U., 2009, Assessment of waste rock weathering characteristics at the Antamina Mine based on field cell experiments. Securing the Future and the 8th ICARD: Proceedings of the conference, Skellefteå, Sweden, pp 211-222.

ASTM, 2013, Standard test method for laboratory weathering of solid material using an humidity cell, ASTM D 5744-13e1.

Bezaazoua, B., Bussieré, B., Dagenais, A.M., Archambault, M., 2004, Kinetic tests comparison and interpretation for prediction of the Joutel tailings acid generation potential. Environmental Geology, 46, pp. 1086-1101

Barazzoul, L., Sexsmith, K., Buckham, C., and Lopex, D., 2012, Application of an Advanced Mineralogical Technique: Sulfide Mineral Availability and Humidity Cell Interpretations based on MLA analysis, 9th International Conference on Acid Rock Drainage: Ottawa, Canada.

Barnes, A., Bowell, R., Warrender, R., Sapsford, D., Sexsmith, K., Charles, J., Declercq, J., Santonastaso, M & Dey, B., 2015, Comparison between Long-Term Humidity Cell Testing and Static Net Acid Generation (NAG) Tests: Potential for NAG Use in Preliminary Mine Site Water Quality Predictions, 10th ICARD & IMWA Annual Conference.

Becker, M., Dyantyi, N., Broadhurst, J.L., Harrison, S.T.L. & Franzidis, J.-P., 2015, A mineralogical approach to evaluating laboratory scale acid rock drainage characterisation tests, Minerals Engineering, 80, pp 33-36

Brough, C.P., Warrender, R., Bowell, R.J., Barnes, A. & Parbhakar-Fox, A., 2013, The process mineralogy of mine wastes, Minerals Engineering, v.52, pp 125-135

EGI (2002). Net Acid Generation (NAG) Test procedures. Environmental Geochemistry International PTY LTD.

Frostad, S., Klein, B., Lawrence, R.W., 2002, Evaluation of laboratory kinetic test methods for measuring rates of waeathering, Mine Water and the Environment, 21, pp 183-192

GARD (Global Acid Rock Drainage) Guide 2014. The international network for Acid Prevention (INAP). http://www.gardguide.com/.

Goodall, W., 2008, Automated mineralogy in the prediction of acid rock drainage: accessible mineralogy using QEMSCAN, Proceedings of the 2008 society for Mining, Metallurgy and Exploration (SME) Annual Meeting and Exhibit: Salt Lake City, Utah, United States.

Lapakko, K.A., 2003, Developments in humidity-cell tests and their application. In: Jambor, J.L., Blowes, D.W., Ritchie, A.I.M. (Eds.), Environmental Aspect of Mine Wastes, Mineralogical Association of Canada, Short Course Series, 31, pp 147 – 164

Lapakko, K.A. and Antonson, D.A., 2006, Pyrite oxidation rates from humidity cell testing of greenstone rock. Paper presented at the 7th ICARD, March 26-30 2006, St Louis, MO

Lehner, S., Savage, K., Ciobanu, M., Cliffel, D.E., 2007, The effect of As, Co and Ni impurities on pyrite oxidation kinetics: an electrochemical study of synthetic pyrite, Geochemica et Cosmochimica Acta, 71, pp 2491 – 2509.

Lehner, S., & Savage, K. 2008, The effect of As, Co and Ni impurities on pyrite oxidation kinetics: batch and flow-through reactor experiments with synthetic pyrite. Geochimica et Cosmochimica Acta 72, pp 1788-1800.

Lottermoser, B.G. 2010, Mine Wastes. Characterisation, Treatment, Environmental Impacts. Third Edition. Berlin-Heidelberg: Springer-Verlag. 400 p.

MEND, (2009), Prediction manual for drainage chemistry from sulfidic geological materials. MEND Report 1.20.1. Report prepared by Price, W.A. December 2009, 579 p.

Nesbitt, H.W., and Jambor, J.L., 1998, Role of mafic minerals in neutralizing ARD, demonstrated using a chemical weathering methodology, in Cabri, L.J., and Vaughan, J.P., eds., Modern approaches to ore and environmental mineralogy, Volume 27, Mineral Association of Canada, pp. 403-421.

Parbhakar-Fox, A.K., Edraki, M., Walters, S., and Bradshaw, D., 2011, Development of a textural index for the prediction of acid rock drainage: Minerals Engineering, v. 24, pp 1277-1287.

Parbhakar-Fox, A.K. Lottermoser, B.G., & Bradshaw, D., 2013, Evaluating waste rock mineralogy and microtexture during kinetic testing for improved acid rock drainage prediction: Minerals Engineering, v. 52, pp 111-124.

Parbhakar-Fox, A.K. & Lottermoser, B.G. 2015, A critical review of acid rock drainage prediction methods and practices: Minerals Engineering, v.82, pp 107-124.

Payant, R., Rosenblum, F., & Nesset, J.E., 2011, Galvanic interaction and particle size effects in self-heating of sulfide mixtures, Materials Science, pp 359-379.

Sapsford, D.J., Bowell, R.J., Dey, M., Williams, K.P., 2009, Humidity cell tests for the prediction of acid rock drainage. Minerals Engineering 22, pp 25–36.

Thornber, M.R., 1993, Electrochemical aspects of sulfide oxidation and environmental implications. In: Proceedings MDSG Annual Meeting, London, December, 15-18, pp 1-12.

Weisener, C.G. & Weber, P.A., 2010. Preferential oxidation of pyrite as a function of morphology and relict texture. New Zealand journal of Geology and Geophysics, 53, pp 22-33.